MAGNETIC RESONANCE IN CHEMISTRY
Magn. Reson. Chem. 2006; **44**: 302–310
Published online in Wiley InterScience (www.interscience.wiley.com). DOI: 10.1002/mrc.1762

MRC

Carbon-13 chemical shift anisotropy in DNA bases from field dependence of solution NMR relaxation rates†

Jinfa Ying,‡ Alexander Grishaev‡ and Ad Bax*

Laboratory of Chemical Physics, National Institute of Diabetes and Digestive and Kidney Diseases, National Institutes of Health, Bethesda, MD 20892, USA

Received 5 October 2005; Revised 27 October 2005; Accepted 28 October 2005

Knowledge of ^{13}C chemical shift anisotropy (CSA) in nucleotide bases is important for the interpretation of solution-state NMR relaxation data in terms of local dynamic properties of DNA and RNA. Accurate knowledge of the CSA becomes particularly important at high magnetic fields, prerequisite for adequate spectral resolution in larger oligonucleotides. Measurement of ^{13}C relaxation rates of protonated carbons in the bases of the so-called Dickerson dodecamer, d(CGCGAATTCGCG)$_2$, at 500 and 800 MHz ^1H frequency, together with the previously characterized structure and diffusion tensor yields CSA values for C5 in C, C6 in C and T, C8 in A and G, and C2 in A that are closest to values previously reported on the basis of solid-state FIREMAT NMR measurements, and mostly larger than values obtained by *in vacuo* DFT calculations. Owing to the noncollinearity of dipolar and CSA interactions, interpretation of the NMR relaxation rates is particularly sensitive to anisotropy of rotational diffusion, and use of isotropic diffusion models can result in considerable errors. Published in 2006 by John Wiley & Sons, Ltd.

KEYWORDS: NMR; ^{13}C; ^1H; base; chemical shift anisotropy; nucleic acid; relaxation

INTRODUCTION

The study of internal dynamics of DNA and RNA by solution NMR is important for developing a better understanding of molecular recognition and is the focus of numerous recent studies.[1–5] The biologically most interesting systems are typically of rather large size by NMR standards (>30–40 nucleotides), and require high magnetic field strengths for optimal resolution. At field strengths corresponding to ^1H frequencies in the 700–900 MHz range, the dipolar and chemical shift anisotropy (CSA) relaxation mechanisms for the protonated ^{13}C nuclei in nucleic acid bases become comparable in size, resulting in relatively large TROSY-enhancements in ^{13}C resolution, in particular, for C2 in A and C5 in U, C, and T nucleotides.[6,7] For quantitative interpretation of the ^{13}C relaxation rates, accurate knowledge of the ^{13}C chemical shift tensors is therefore a prerequisite. In previous studies, a substantial range of CSA values has been used, differing by as much as 30% for a given site, with experimentally determined CSA on average being higher than computed values.[5,8–12] In the model compound pyrimidine, relatively large ^{13}C CSA values, close to the highest values used in NMR relaxation studies, were observed by magic-angle spinning liquid-crystal NMR.[13] The most complete chemical shift tensors were reported relatively recently for the full set of deoxyribose mononucleotides.[10] These data were based on slow-magic-angle spinning samples using the solid-state FIREMAT NMR method, with orientations of the tensors obtained from density-functional theory (DFT) calculations. Considerable impact of the electrostatic crystal potentials were shown in this work, suggesting that some adjustment of the CSA values may be required in hydrated Watson–Crick base-paired oligonucleotides.

To date, most NMR relaxation studies have focused on a small subset of the potentially accessible ^{13}C–{^1H} sites in oligonucleotides. Any small deviation of the applicable CSA during interpretation of the NMR data primarily manifests itself as a change in the derived order parameters. In a recent report, Duchardt and Schwalbe simultaneously analyze relaxation data of all protonated base carbons in both purines and pyrimidines of a small hairpin RNA.[14] They find that the use of literature CSA values leads to the remarkable result of systematically lower-order parameters for purine C8 compared to pyrimidine C6 sites, even for base-paired nucleotides. They also report that relaxation data recorded for ^{15}N and ^{13}C in the same nucleotide point to a mismatch in the commonly used CSA values, and raise the question whether CSA values in solution NMR require adjustment from values commonly used.

Closely related to the applicable CSA values is the question of which internuclear C–H or N–H bond length to

†Dedicated to Professor David M. Grant of the University of Utah on the occasion of his 75th birthday, in recognition of the outstanding contributions he has made to the methodology of nuclear magnetic resonance and its application to a wide range of chemical topics over a long period of time.

*Correspondence to: Ad Bax, Laboratory of Chemical Physics, Building 5, Room 126, NIDDK, National Institutes of Health, Bethesda, MD 20892, USA. E-mail: bax@nih.gov
‡These authors contributed equally.

use in NMR relaxation analyses. When analyzing either solution or solid-state NMR data, the ultrafast internal motions, related to bond librations and vibrations, manifest themselves as reduced interactions in solids, and a reduction in $J(0)$ spectral density term in liquids. For example, the dipolar couplings observed in solid-state NMR for one-bond $^{15}N-^{1}H$ and $^{13}C-^{1}H$ interactions correspond to distances that are approximately 2–3% longer than observed by neutron scattering.[15–18] For CSA, it is not possible to evaluate quantitatively the effect of ultrafast motions as all solid-state NMR spectra incorporate these effects.

It remains common practice in NMR relaxation analyses to use the static, nonvibrationally corrected bond lengths. Although this leads to a theoretical upper limit for the generalized order parameter, $S^2 \approx 0.9$,[16] it avoids the appearance of physically impossible $S^2 > 1$ values that often would occur as a result of small measurement errors when using the vibrationally corrected, effective bond length for calculating the dipolar interaction constant. However, considering that in the solid state the effect of ultrafast motions is imposed on both the dipolar interaction and on the observed CSA powder pattern, it is important that when these values are used in the analysis of solution NMR data, the vibrationally corrected bond lengths are used. In the case of ^{15}N, this means that a vibrationally corrected 1.04-Å N–H bond length should be paired with the 160-ppm ^{15}N CSA,[19] observed by solid-state NMR. Alternatively, if one maintains a 1.02-Å N–H bond length to avoid occasional $S^2 > 1$ values, the CSA needs to be scaled up to 170 ppm too. Similarly, when using the solid-state NMR-derived ^{13}C CSA values, vibrationally corrected bond distances need to be used, or solid-state CSA values need to be scaled up. Previous liquid-crystal NMR experiments indicate an r_{CH} increase by *ca* 2.3% over standard bond lengths.[18] Instead of the commonly used 1.08-Å C–H distance in aromatic systems, we therefore use a vibrationally corrected value of 1.104 Å for the base carbons.

EXPERIMENTAL SECTION

NMR measurements were carried out at 500 and 800 MHz ^{1}H frequency, 25 °C, using Bruker DRX model consoles, equipped with cryogenic *z*-gradient inverse triple resonance probeheads. Additionally, 800 MHz measurements of transverse ^{13}C relaxation rates, $R_2(C_+^{(\alpha)})$ and $R_2(C_+^{(\beta)})$, where the superscripts correspond to the spin state of the directly attached ^{1}H, were carried out at 15 °C in order to ensure that no significant conformational exchange contributions were present in the measurements carried out at 25 °C. Special care was taken to ensure that the effective sample temperature on the 500- and 800-MHz spectrometers was not affected by thermocouple calibration or radio frequency heating. The NMR sample consisted of a 2.5 mM $d(CGCGAATTCGCG)_2$ (5 mM monomer) in D_2O, 50 mM KCl, 1 mM EDTA, 0.02% NaN_3, 10 mM sodium phosphate buffer, pH 7.0 (apparent meter reading).

Measurements of the relaxation rates $R_2(C_+^{(\alpha)})$, $R_2(C_+^{(\beta)})$, $R_1(C_z)$, and $R_1(C_zH_z)$ were carried out using standard pulse sequences.[7,20] Typical data acquisition times were 2 days for each measurement. Spectra were processed and analyzed with NMRPipe software.[21]

Measurements of $^{13}C-\{^{1}H\}$ NOE values were carried out with the pulse scheme of Fig. 1. Relative to conventional measurements, which require a delay time between transients equal to at least three times the longest ^{1}H T_1 values in the molecule,[22] our implementation reduces the typically lengthy acquisitions. In natural abundance ^{13}C nucleic acid samples, ^{1}H T_1 values are typically very long, up to 8 s at 800 MHz for the A-C2 ^{1}H and *ca* 5–6 s for most others, whereas ^{13}C T_1 values are much shorter (Table 1). Immediately prior to the start of acquisition, the pulse scheme of Fig. 1 flips back to *z* the ^{1}H magnetization for sites not attached to ^{13}C, rather than waiting for protons to recover through T_1 relaxation. In the absence of any losses resulting from relaxation or pulse imperfections, 98.9% of all ^{1}H magnetization would be recovered in this manner. In practice, we obtain an ~80% recovery. Subsequently, magnetization from

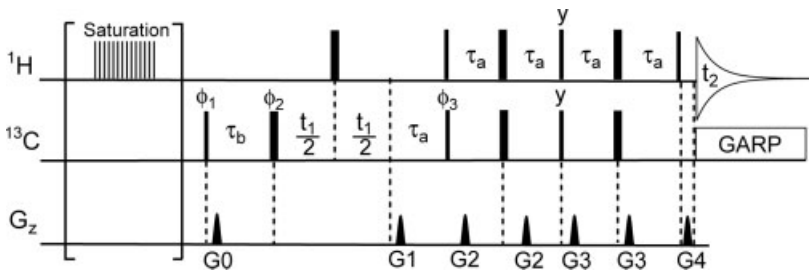

Figure 1. Pulse sequence for gradient-enhanced measurement of $\{^{1}H\}-^{13}C$ NOEs, closely similar to that of Kay and coworkers.[23] Narrow bars and wide bars represent 90° and 180° pulses respectively. Unless otherwise indicated, all pulses have phase *x*. In the NOE experiment, a train of 120° ^{1}H pulses spaced at 50-ms intervals for 3 s at 500 MHz and 4 s at 800 MHz is applied to saturate protons prior to the first ^{13}C pulse. In the reference experiment without NOE, a delay of identical total duration is used. To benefit from the flip-back to *z* of ^{12}C-attached ^{1}H magnetization, the reference and saturated experiments cannot be interleaved. Other delays: $\tau_a = 1.2$ ms; $\tau_b = \tau_a + 2 \times$ pw, where pw is the duration of the ^{1}H 90° pulse. Phase cycling: $\phi_1 = y$; $\phi_2 = x, y, -x, -y$; $\phi_3 = x$; receiver $= x, -x$. Pulse phases refer to Bruker spectrometers. Quadrature detection is achieved by inverting the phase ϕ_3 and the amplitude of the G0 and G1 gradient pulses for the second FID in each t_1 increment. To shift the axial peak to the edge of the spectrum, ϕ_1 and the receiver phase are incremented by 180° for each t_1 increment. Pulsed field gradients are sine-bell shaped with durations of 100 μs for G0 and G1, 500 μs for G2 and G3, and 50.6 μs for G4. The peak amplitudes of the gradient pulses G0–G4 are −21, 27, 3.6, 1.8, and 24 Gcm^{-1} respectively.

MRC

Table 1. Relaxation rates (s^{-1}) and steady-state NOEs for d(CGCGAATTCGCG)$_2$

		500 MHz			800 MHz			
Carbon	Nucleotide	$R_2(C_+)$	$R_1(C_z)$	NOE	$R_2(C_+^{(\beta)})$	$R_2(C_+^{(\alpha)})$	$R_1(C_z)$	NOE
C2	A5	28.8	2.64	1.20	9.1	75.8	1.41	1.18
	A6	28.3	2.63	1.20	8.2	76.7	1.46	1.21
C5	C1	22.2	2.38	–	7.2	51.5	1.45	–
	C3	26.1	2.59	–	6.6	63.7	1.38	–
	C9	24.7	2.55	–	6.3	65.2	1.47	–
	C11	24.3	2.66	–	6.5	62.9	1.53	–
C6	C1	25.9	2.74	1.32	14.2	67.2	1.75	1.30
	C3	30.1	2.86	1.22	16.4	80.6	1.74	1.14
	T7	30.4	2.80	1.20	14.6	78.9	1.56	1.13
	T8	29.8	2.79	1.24	13.9	79.0	1.60	1.12
	C9	29.6	2.88	1.29	15.5	78.9	1.81	1.19
	C11	30.4	2.88	1.28	14.9	76.8	1.77	1.17
C8	G2	25.1	2.46	1.34	11.3	55.1	1.45	1.28
	G4	26.0	2.69	1.20	10.7	55.8	1.35	1.18
	A5	27.1	2.54	1.24	12.5	60.2	1.36	1.18
	A6	26.2	2.55	1.25	12.7	59.8	1.37	1.16
	G10	24.9	2.67	1.27	11.3	55.8	1.43	1.24
	G12	23.2	2.48	1.33	10.1	51.2	1.40	1.36
Estimated error		0.6	0.06	0.03	0.2	1.5	0.04	0.03

^{13}C-attached protons equilibrates rapidly with those of the bulk ^{12}C-attached protons through spin diffusion. The delay between transients is subsequently adjusted such that under steady-state conditions the ^{1}H spin polarization has reached 80% of its equilibrium value, requiring 4 s at 800 MHz and 3 s at 500 MHz. The steady-state value is monitored by acquiring a single FID with a 90° ^{1}H pulse inserted just prior to acquisition, preceded by 8 dummy scans without this pulse, and comparing the corresponding spectrum to that obtained for a 90° ^{1}H pulse applied to a fully relaxed sample. Note that the spectra with and without ^{1}H NOE cannot be recorded in the usual interleaved manner when using the flip-back feature, and instead are recorded sequentially. ^{13}C intensity in the spectrum with ^{1}H saturation is $1+\varepsilon$, where ε denotes the change resulting from the NOE. In the reference spectrum, where ^{1}H spin magnetization is 80% recovered, ^{13}C intensity is $1+0.2\times\varepsilon$, then allowing the value of ε to be determined from the measured ratio $(1+\varepsilon)/(1+0.2\varepsilon)$. Values reported in Table 1 have been adjusted in this manner for the 20% ^{1}H saturation in the spectrum recorded nominally without NOE.

RESULTS AND DISCUSSION

The ^{13}C relaxation rates for an isolated ^{13}C–^{1}H spin pair can be expressed as

$$R(C_+^{(\alpha)}) = [R(C_+) + R(C_+H_z)]/2 + \Gamma_{C,CH} \quad (1a)$$

$$R(C_+^{(\beta)}) = [R(C_+) + R(C_+H_z)]/2 - \Gamma_{C,CH} \quad (1b)$$

where, for an anisotropic rotor, the CSA and dipolar contributions to $R(C_+)$, as well as expressions for the longitudinal relaxation rates, $R(C_z)$ and $R(H_z)$, are given by Spiess.[24,25] To a first approximation, the differences between in-phase and anti-phase relaxation in the presence of remote protons, not J coupled to the ^{13}C of interest, are given by

$$R(C_+) - R(C_+H_z) = (3/4)\xi^2_{DD} J(\omega_H) - \rho_{HH} \quad (2a)$$

$$R(C_z) - R(C_zH_z) = (1/4)\xi^2_{DD}\,[J(\omega_H - \omega_C) - 3J(\omega_H) + 6J(\omega_H + \omega_C)] - \rho_{HH} \quad (2b)$$

with

$$\xi_{DD} = (\mu_0/4\pi)(h/2\pi)\gamma_C\gamma_H\langle r_{CH}^{-3}\rangle$$

and ρ_{HH} being the ^{1}H selective longitudinal relaxation rate in the absence of the attached ^{13}C. In the macromolecular limit, ρ_{HH} is dominated by $J(0)$ multiplied by homonuclear ^{1}H–^{1}H dipolar interactions.[26] Therefore, to a good approximation, $R(C_+H_z) - R(C_+) \approx \rho_{HH} \approx R(C_zH_z) - R(C_z)$, and the latter is readily measured.[20] Under this approximation,

$$R(C_+) \approx [R(C_+^{(\alpha)}) + R(C_+^{(\beta)})]/2 + [R(C_z) - R(C_zH_z)]/2 \quad (3)$$

The cross-correlation term, $\Gamma_{C,CH}$, in Eqn 1 can readily be calculated from the difference in the $R^{CSA}(C_+)$ values calculated for two 'pseudo-CSA' tensors, corresponding to the sum and the difference of the regular ^{13}C chemical shift tensor and the tensor describing the dipolar field of the ^{1}H at the position of the ^{13}C. The latter has the same form as an axially symmetric chemical shift tensor, with its unique axis parallel to the C–H bond, and $\delta_{ZZ} = (1/\omega_C)\,(\mu_0/4\pi)\,(h/2\pi)\,\gamma_C\gamma_H\langle r_{CH}^{-3}\rangle$. Transverse relaxation rates are then calculated with the general expressions of Spiess:[24,25]

$$R^{CSA}(C_+) = (1/2)\omega_C^2[g_2(\omega) + (4/3)g_2(0)] \quad (4a)$$

with ω_C being the angular ^{13}C Larmor frequency, and

$$g_2(\omega) = \Sigma_{k=-2,\ldots,2} c_k[S^2\tau_k/(1+\omega^2\tau_k{}^2) + (1-S^2\tau_e)/(1+\omega^2\tau_e{}^2)] \quad (4b)$$

Here,

$$1/\tau_e = 1/\tau_k + 1/\tau_f \quad (4c)$$

with τ_f being the effective correlation time for fast internal motion, and S^2 the generalized Lipari–Szabo order parameter.[27] The coefficients, c_k, depend on the 'pseudo-CSA' tensor and its orientation relative to the diffusion tensor:

$$c_{-2} = (\delta_{ZZ}{}^2/40)\{3\ \sin^2\beta\ \sin\ 2\gamma - \eta[\cos 2\alpha\ \sin\ 2\gamma \times (\cos^2\beta + 1) + 2\ \sin\ 2\alpha\ \cos\ 2\gamma\ \cos\ \beta]\}^2 \quad (5a)$$

$$c_{-1} = (\delta_{ZZ}{}^2/40)\{3\ \sin\ 2\beta\ \cos\ \gamma + \eta[\cos\ 2\alpha\ \sin\ 2\beta\ \cos\ \gamma - 2\ \sin\ 2\alpha\ \sin\ \beta\ \sin\ \gamma]\}^2 \quad (5b)$$

$$c_0 = \{\delta_{ZZ}{}^2/[60A(1+A)]\}\{(3/2)(1+A)\ (3\ \cos^2\beta - 1 - \eta\sin^2\beta\ \cos\ 2\alpha) - (\kappa/2)[3\ \sin^2\ \beta\cos\ 2\gamma - \eta(\cos\ 2\alpha\ \cos\ 2\gamma(\cos^2\ \beta + 1) - 2\ \sin\ 2\alpha\ \sin\ 2\gamma\ \cos\ \beta)]\}^2 \quad (5c)$$

$$c_1 = (\delta_{ZZ}{}^2/40)\{3\ \sin\ 2\beta\ \sin\ \gamma + \eta[\cos\ 2\alpha\ \sin\ 2\beta\ \sin\ \gamma + 2\ \sin\ 2\alpha\sin\ \beta\ \cos\ \gamma]\}^2 \quad (5d)$$

$$c_2 = \{\delta_{ZZ}{}^2/[20A(1+A)]\}\{-(\kappa/2)\ (3\ \cos^2\beta - 1 - \eta\sin^2\beta\ \cos\ 2\alpha) + [(1+A)/2][3\ \sin^2\ \beta\ \cos\ 2\gamma - \eta(\cos\ 2\alpha\ \cos\ 2\gamma(\cos^2\ \beta + 1) - 2\ \sin\ 2\alpha\sin\ 2\gamma\ \cos\ \beta)]\}^2 \quad (5e)$$

where α, β, and γ are the Euler angles for rotating the 'pseudo-CSA' principal axis system to that of the diffusion tensor, and the asymmetry, $\eta = (\delta_{YY} - \delta_{XX})/\delta_{ZZ}$, with δ_{XX}, δ_{YY}, and δ_{ZZ} being the principal components of the pseudo-CSA tensor. The time constants, τ_k, in Eqn 4 are given by

$$\tau_{-2} = (6D_S)^{-1}[1 + D^*/(2D_S)]^{-1} \quad (6a)$$

$$\tau_{-1} = (6D_S)^{-1}[1 - D^*(1-\kappa)/(4D_S)]^{-1} \quad (6b)$$

$$\tau_0 = (6D_S)^{-1}[1 - D^*A/(2D_S)]^{-1} \quad (6c)$$

$$\tau_1 = (6D_S)^{-1}[1 - D^*(1+\kappa)/(4D_S)]^{-1} \quad (6d)$$

$$\tau_2 = (6D_S)^{-1}[1 + D^*A/(2D_S)]^{-1} \quad (6e)$$

with $D_S = (D_{XX} + D_{YY} + D_{ZZ})/3$ and D_{XX}, D_{YY}, and D_{ZZ} being the principal components of the rotational diffusion tensor; $D^* = D_{ZZ} - D_S$; $\kappa = (D_{YY} - D_{XX})/D^*$; $A = (1 + \kappa^2/3)^{1/2}$. Together with the previously reported equations for $R_1{}^{DD}$, $R_1{}^{CSA}$, $R_2{}^{DD}$, and $R_2{}^{CSA}$ as well as $\Gamma_{C,CH}$, it is then straightforward to calculate the auto and cross-correlated relaxation times for a known structure and a given diffusion tensor. We apply this approach to the palindromic DNA dodecamer, $d(CGCGAATTCGCG)_2$, also known as the *Dickerson dodecamer*, previously studied extensively by X-ray crystallography and NMR.

Absence of conformational exchange

The presence of conformational exchange on a timescale slower than the overall rotational correlation time of the molecule, but fast on the chemical shift timescale is always a major concern when analyzing macromolecular relaxation data. This type of process contributes a so-called exchange term, R_{ex}, to both $R_2(C_+{}^{(\beta)})$ and $R_2(C_+{}^{(\alpha)})$, but does not affect the relaxation interference term, $\Gamma_{C,CH}$. In the fast-exchange limit, R_{ex} scales with the square of the magnetic field strength:

$$R_{ex} = p_A p_B(\delta\omega)^2/k_{ex} \quad (7)$$

where p_A and p_B are the populations of conformers A and B, $\delta\omega$ is the angular frequency difference between states A and B and $k_{ex} = p_B/k_{A\to B} = p_A/k_{B\to A}$. Assuming that any process that gives rise to a microsecond conformational exchange process is likely to have an activation energy $E_A \geq 40$ kJ mol^{-1}, one expects at least a 1.8-fold decrease in k_{ex} when lowering the temperature by 10 °C, whereas fractional changes in p_A and p_B will be small. Therefore, the presence of conformational exchange leads to an R_{ex} contribution that is increased at least 1.8-fold when lowering the sample temperature by 10 °C and should be easily recognized if significant.

R_{ex} contributes equally to $R_2(C_+{}^{(\alpha)})$ and $R_2(C_+{}^{(\beta)})$. However, considering the much lower intrinsic values of $R_2(C_+{}^{(\beta)})$, they are far more sensitive to R_{ex} contributions than $R_2(C_+{}^{(\alpha)})$. The expected change with temperature for any R_{ex} contribution therefore should manifest itself in a decrease of the ratio $\zeta = R_2(C_+{}^{(\alpha)})/R_2(C_+{}^{(\beta)})$ at lower temperature. No statistically significant decrease in ζ at 15 °C relative to 25 °C was found for any of the base carbons, however. Similarly, when comparing $R_2(C_+{}^{(\beta)})^{15C}$ with $R_2(C_+{}^{(\beta)})^{25C}$, no outliers are seen (Fig. 2), indicating the absence of detectable R_{ex} contributions.

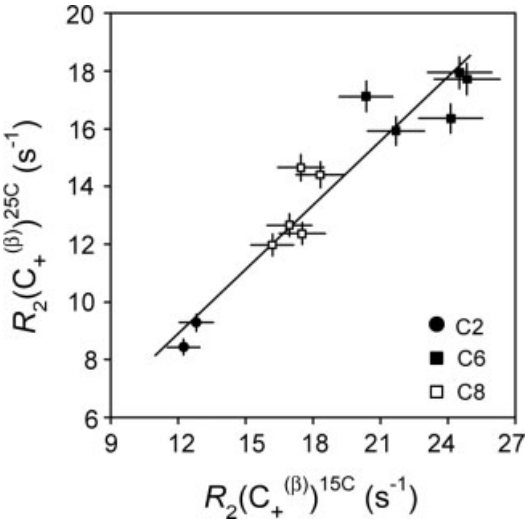

Figure 2. Comparison of ^{13}C TROSY relaxation rates at 15 °C and 25 °C. The good correlation ($R^2 = 0.90$) and the absence of outliers indicates the absence of detectable R_{ex} contributions.

Estimation of diffusion rate

Both, hydrodynamic modeling and analysis of experimental measurement of deoxyribose ^{13}C relaxation times, yield an axially symmetric ($\kappa = 0$; $A = 1$) diffusion tensor, with an anisotropy $D_{//}/D_{\perp} = 2.1 \pm 0.4$.[28] A search over D_S values was conducted to find best agreement between measured and calculated R_2/R_1 ratios, taking literature CSA values of Stueber and Grant,[10] and three different $D_{//}/D_{\perp}$ ratios (Fig. 3). The terminal base pairs (C1–G24; G12–C13), which are subject to increased internal dynamics, as judged by slightly elevated $^{13}C-\{^1H\}$ NOE and increased T_2 values (Table 1), were excluded from this analysis. Data collected at 500 and 800 MHz ^1H frequency yield an effective correlation time, $\tau_c = 1/(6D_S) = 5.0$ ns, which is about 10% longer than expected on the basis of data previously recorded at 35 °C,[28] a difference attributed to the sixfold higher sample concentration used in the present study.

The derived τ_c is not particularly sensitive to the precise value of the CSA: increasing all CSA values by 10% over those of Stueber and Grant decreases τ_c by only 1.2%. The anisotropy of the diffusion tensor cannot be extracted at reasonable accuracy from the base ^{13}C relaxation rates because the distribution in orientations of the corresponding $^{13}C-^1H$ interactions relative to the helix axis is too narrow. Instead, the previously fitted axially symmetric anisotropic diffusion model, with $D_{//}/D_{\perp} = 2.1$, is used here.[28] This degree of diffusion anisotropy agrees closely with results from hydrodynamic modeling.

Magnitude of ^{13}C CSA

The combination of relaxation times, $2R_2 - R_1$, is dominated by $J(0)$ spectral density terms[30] and therefore is particularly well suited for determination of the magnitude of the chemical shift tensor. In such an analysis, however, it is critical that the anisotropy of the diffusion tensor is taken into account. For example, Fig. 4 shows the $^{13}C2$ CSA magnitude, $|\delta| = (\delta_x^2 + \delta_y^2 - \delta_x\delta_y)^{1/2}$, where $\delta_x = \delta_{XX} - \delta_{ZZ}$ and $\delta_y = \delta_{YY} - \delta_{ZZ}$, as a function of the diffusion anisotropy. Parenthetically, we note that this commonly used notation is equivalent to $|\delta| = (1/2)[(2\delta_{ZZ} - \delta_{XX} - \delta_{YY})^2(1 + \eta^2/3)]^{1/2}$, often used in solid-state NMR literature. In Fig. 4, the asymmetry, $\eta = (\delta_{YY} - \delta_{XX})/\delta_{ZZ}$, and angle θ between the δ_{XX} axis and the C–H bond, are fixed at the values reported by Stueber and Grant.[10] Neglecting diffusion anisotropy in the analysis for the Dickerson dodecamer would result in an overestimate of $|\delta|$ by about 23 ppm. It is also interesting to note that even a relatively small diffusion anisotropy already has a large effect on the extracted value of $|\delta|$. Figure 5(A) plots the agreement between observed ratios of $(2R_2 - R_1)^{500\ MHz}/(2R_2 - R_1)^{800\ MHz}$ and the ratios computed on the basis of the above derived diffusion tensor values, using Stueber-and-Grant CSA values. The error bars in the computed ratios correspond to the range computed for diffusion anisotropies, $D_{//}/D_{\perp}$, ranging from 1.7 to 2.5. As can be seen from the figure, agreement is very good for the C8 carbons, but the discrepancies tend to be systematically larger, on average, for the other types of carbons, in particular, for adenine C2 and pyrimidine C5.

Although for an isotropically tumbling molecule $|\delta|$ is uniquely related to the field dependence of $2R_2 - R_1$, for an anisotropically diffusing system, this simplification does not apply. For example, as can be seen in Fig. 5(A), ratios computed for a given type of ^{13}C vary slightly for the different sites in the molecule and depend on the orientation of the corresponding base relative to the z-axis of the diffusion tensor. Unfortunately, the spread in orientations of the base normals relative to the helical axis of this DNA dodecamer is rather small, and is insufficient to reliably extract all three unknowns of the chemical shift tensor from the two observables, $(2R_2 - R_1)^{500\ MHz}/(2R_2 - R_1)^{800\ MHz}$ and

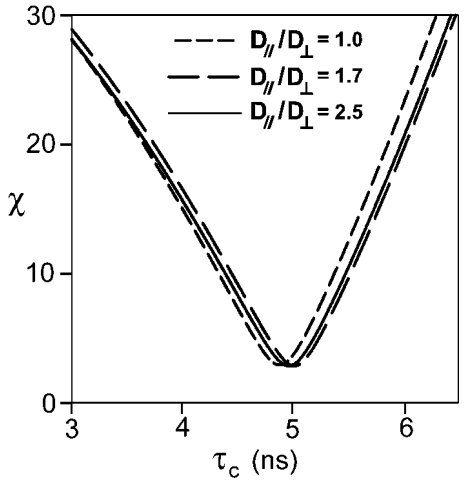

Figure 3. Normalized error (χ) as a function of the effective rotational correlation time, $\tau_c = (6D_S)^{-1}$, when fitting R_2/R_1 ratios of the base carbons (Table 1) to the structure of $d(CGCGAATTCGCG)_2$, ignoring internal motions, and excluding the terminal base pairs (PDB code 1NAJ).[29] Search results are shown for three different degrees of axially symmetric diffusion anisotropy: $D_{//}/D_{\perp} = 1.0$, 1.7, and 2.5.

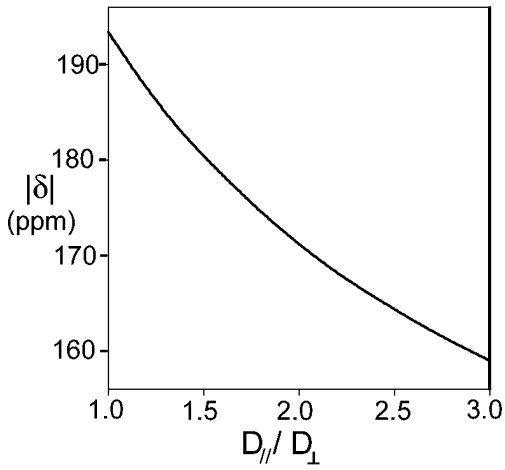

Figure 4. Dependence of the best-fitted adenine C2 $|\delta|$ on the anisotropy of the rotational diffusion tensor while keeping $\tau_c = (6D_S)^{-1} = 5.0$ ns, when simultaneously fitting $(2R_2 - R_1)^{500\ MHz}/(2R_2 - R_1)^{800\ MHz}$ and $R_2{}^{800\ MHz}/\Gamma^{800\ MHz}$ of nucleotides A5 and A6. The angle θ between δ_{XX} and the C2–H bond, and the asymmetry, η, of the chemical shift tensor are kept fixed at the Stueber-and-Grant values.

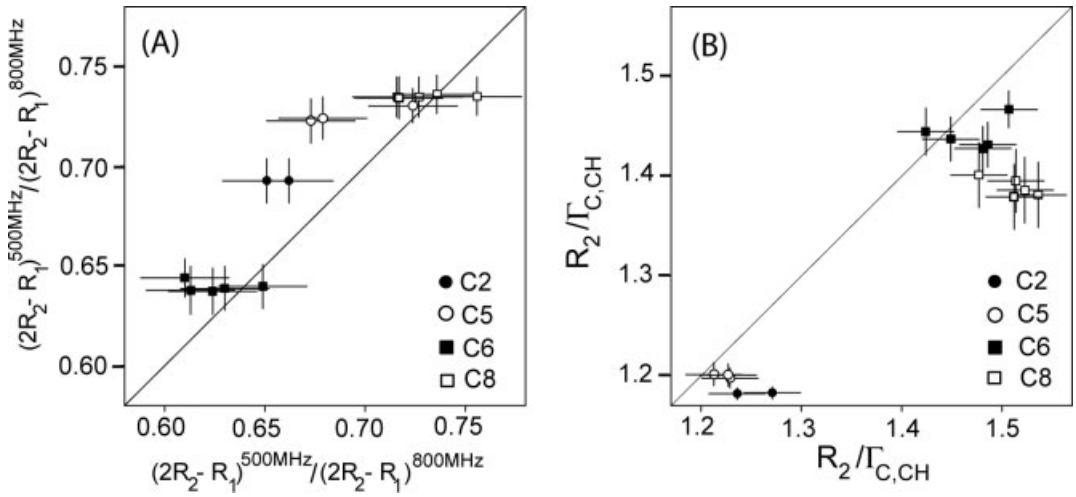

Figure 5. Comparison of observed (horizontal) and calculated relaxation parameters. (A) Ratio of $2R_2 - R_1$ at 500 MHz and 800 MHz for each of the base carbons in the dodecamer, except for terminal base pairs. (B) Ratio of $R_2/\Gamma_{C,CH}$ at 800 MHz ^{1}H frequency. Calculated ratios are derived for chemical shift tensor values of Stueber-and-Grant for $\tau_c = 5.0$ ns and $D_{///}/D_\perp = 2.1$. Horizontal error bars correspond to propagated experimental uncertainties; vertical error bars delineate the $D_{///}/D_\perp = 1.7$–2.5 range.

$R_2{}^{800}/\Gamma_{C,CH}{}^{800}$, available for each carbon in the differently oriented bases.

Figure 6(A) shows the agreement between our experimental $(2R_2 - R_1)^{500\ MHz}/(2R_2 - R_1)^{800\ MHz}$ ratios and values computed for a C2 chemical shift tensor as a function of $|\delta|$ and η, when keeping the angle θ, between the δ_{XX} axis and the C–H bond, fixed at $-3°$. Under the condition of axially symmetric diffusion, when η is kept fixed, $|\delta|$ is nearly independent of θ, however, (Fig. 6(B)). Parenthetically, we note that for nucleic acid bases, with the z-axis defined orthogonal to the plane of the base, the angle between δ_{ZZ} and the C–H bond is 90°, and is not assigned a separate symbol.

Relaxation interference

With the known structure and diffusion tensor, values for $\Gamma_{C,CH}$ are computed using Eqns 4–6, and values for the transverse relaxation rate are obtained using the equations of Spiess.[24] Fig. 5(B) shows that the agreement between computed and experimentally observed $R_2/\Gamma_{C,CH}$ ratios is close for C5 and C6 carbons, but a slightly larger than expected ratio is observed for C2 and, in particular, C8.

Under isotropic tumbling, $\Gamma_{C,CH}$ contains a term proportionate to $3\cos^2\theta - 1$, where θ is the angle between the δ_{XX} axis and the C–H bond. Under anisotropic diffusion, the expressions for $\Gamma_{C,CH}$ are more complex (Eqn 4). Nevertheless, qualitatively, the dependence on θ remains strongest when it approaches 45°. No experimental data on θ are available for any of the carbons, and computed orientations are influenced by electric field effects. With a relatively large θ angle of 27°, $\Gamma_{C,CH}$ for C8 carbons is not only quite sensitive to small adjustments to this angle but is also sensitive to the asymmetry of the chemical shift tensor, η.

The $R_2/\Gamma_{C,CH}$ ratio is relatively sensitive to the asymmetry of the chemical shift tensor. For example, Fig. 6(C) illustrates for adenine C2 carbons that when keeping the value of θ fixed at the Stueber-and-Grant value of $-3°$, the difference between observed and calculated $R_2/\Gamma_{C,CH}$ values can be satisfied over a wide range of $|\delta|$, but requires that η remains close to 0.8. On the other hand, when fixing η at the Stueber-and-Grant value of 0.92, θ depends strongly on the precise value of $|\delta|$ (Fig. 6(D)). The sign of θ remains ill defined, with the agreement between observed and calculated data being largely symmetrical around the $\theta = 0$ line. Note that this symmetry would be broken if the difference in orientations of the two adenine bases relative to the unique axis of the diffusion tensor were sufficiently large. However, in the Dickerson dodecamer, both normals to the A bases are at very similar angles relative to this axis (12.9° and 12.4°), prohibiting determination of the sign of θ.

Simultaneous fit of $\Gamma_{C,CH}$ and field dependence of R_2

As pointed out above, our data are insufficient to uniquely define $|\delta|$, η, and θ. The $R_2/\Gamma_{C,CH}$ data alone can only place broad limits on the C2 CSA: $|\delta|$ between 92 and 243 ppm and the θ angle between $-22°$ and $+22°$ at a 99% confidence level. Similarly, the field dependence of $(2R_2 - R_1)$ can be satisfied over a considerable range of η and θ values. However, the $R_2/\Gamma_{C,CH}$ and $(2R_2 - R_1)^{500\ MHz}/(2R_2 - R_1)^{800\ MHz}$ experimental restraints on the chemical shift tensor are highly complementary, and together provide reasonably tight restrictions on the applicable ^{13}C chemical shift tensor values.

Figure 7 shows orthogonal cross sections through the three-dimensional $|\delta|$, η, θ space, showing the regions where simultaneous agreement between observed and calculated $R_2/\Gamma_{C,CH}$ and $(2R_2 - R_1)^{500\ MHz}/(2R_2 - R_1)^{800\ MHz}$ values is obtained within 1, 2, or 3 standard deviations; the latter corresponding to the 99% confidence interval. The orthogonal cross sections are taken at values of η and θ that correspond to the Stueber-and-Grant values. As can be seen by comparing the left and center panels, the $|\delta|$ values for best agreement between observed and calculated data are very similar for A-C2 as well as for pyrimidine C5 and C_6 carbons.

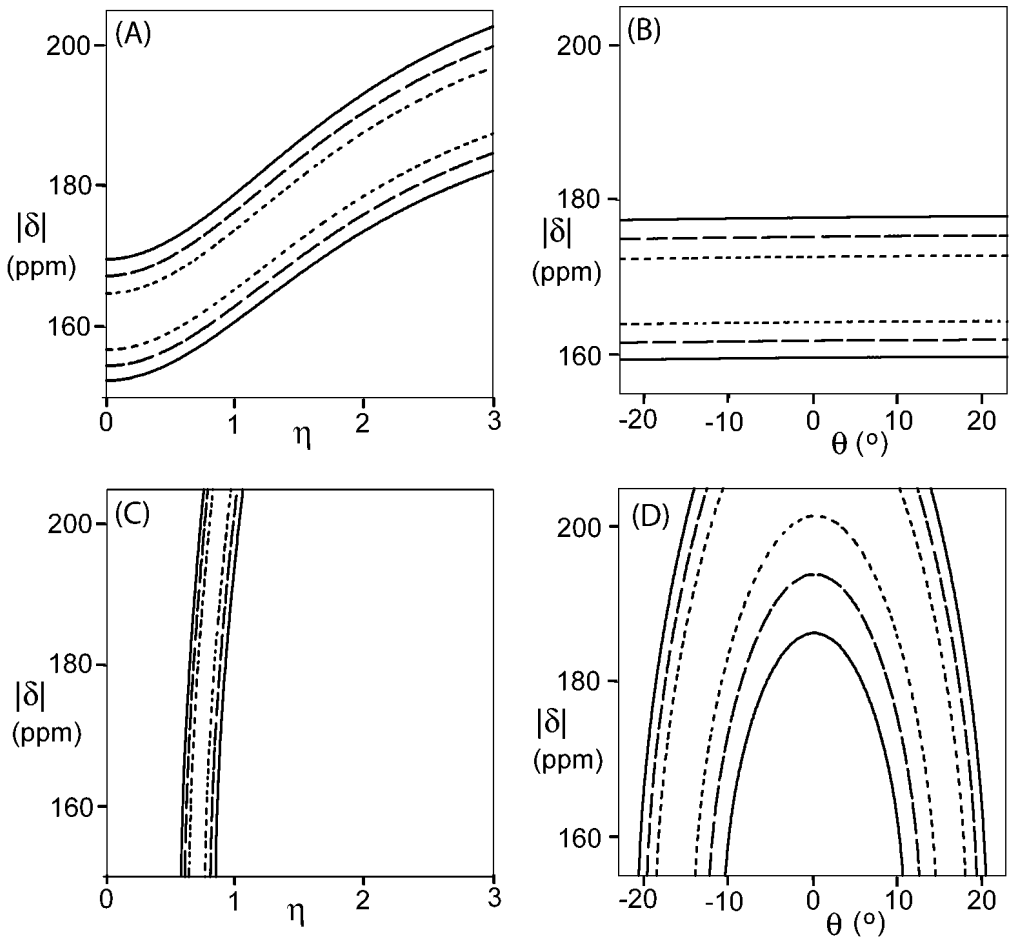

Figure 6. Agreement between experimental and calculated relaxation parameters for adenine C2, as functions of the ^{13}C CSA magnitude $|\delta|$, asymmetry η, and the δ_{XX}/C–H bond angle, θ, assuming for $\tau_c = 5.0$ ns and $D_{///}/D_{\perp} = 2.1$. Short-dashed, long-dashed, and solid contour lines are drawn at normalized χ values that are 1, 2, and 3 standard deviations above the minimum respectively. The error surface corresponds to that of the sum of nucleotides A5 and A6. Panels (A) and (B) show the agreement between the experimental and calculated $(2R_2 - R_1)^{500\ MHz}/(2R_2 - R_1)^{800\ MHz}$ ratios when (A) fixing $\theta = -3°$, and (B) $\eta = 0.92$. (C) and (D) are the analogous plots when evaluating the agreement between observed and calculated $R_2/\Gamma_{C,CH}$ values. The values $\theta = -3°$ and $\eta = 0.92$ are taken from Stueber-and-Grant.[10]

Only for C8 is there a slight difference in $|\delta|$ when comparing the $|\delta|$, θ plot with the $|\delta|$, η plot (Fig. 7(D)). Comparison of the center and right panels shows the close coupling between the θ angle and the asymmetry of the chemical shift tensor. So, even though the left and center panels for C8 suggest much smaller values for η than seen in the solid state, the right-hand panel for C8 shows that the $\eta = 1.02$ value of Stueber and Grant is easily satisfied by a very small increase in the angle θ. Interestingly, Stueber and Grant report that the asymmetry and precise orientation of the δ_{yy} component are very sensitive to electric field effects, which are quite different for the oligonucleotide in aqueous solution studied here, polycrystalline mononucleotides, and *in vacuo* computations. For C5 and C6 sites, the 95% confidence interval of our data includes the $|\delta|$, η, and θ values derived from solid-state NMR. Only for C2 is there an increase in $|\delta|$ that exceeds the uncertainty of our measurement, and a difference in either η or θ (or both) is required to attain a satisfactory agreement with our relaxation data. The larger difference relative to solid-state mononucleotide data, observed for C2, is perhaps not surprising considering that the carbon is adjacent to a nitrogen that is involved in Watson–Crick base pairing in the Dickerson dodecamer, whereas such base paring is not possible in polycrystalline mononucleotides, and no hydrogen bonding is considered in the quantum computations.

CONCLUDING REMARKS

Extraction of chemical shift tensor information from the simultaneous analysis of the field dependence and cross-correlation relaxation rates relies on the premise that all carbons of a given type have identical chemical shift tensors. On the basis of the narrow distributions of isotropic chemical shifts for each type of carbon, with maximum variations of at most 5.3 ppm, this is expected to be a reasonable, albeit not perfect, approximation for the regular B-form nucleotides considered in this study. However, considering that the isotropic shifts of nucleotides in different geometries can deviate substantially from these values, it is conceivable that their chemical shift tensors components will deviate substantially from the results presented here.

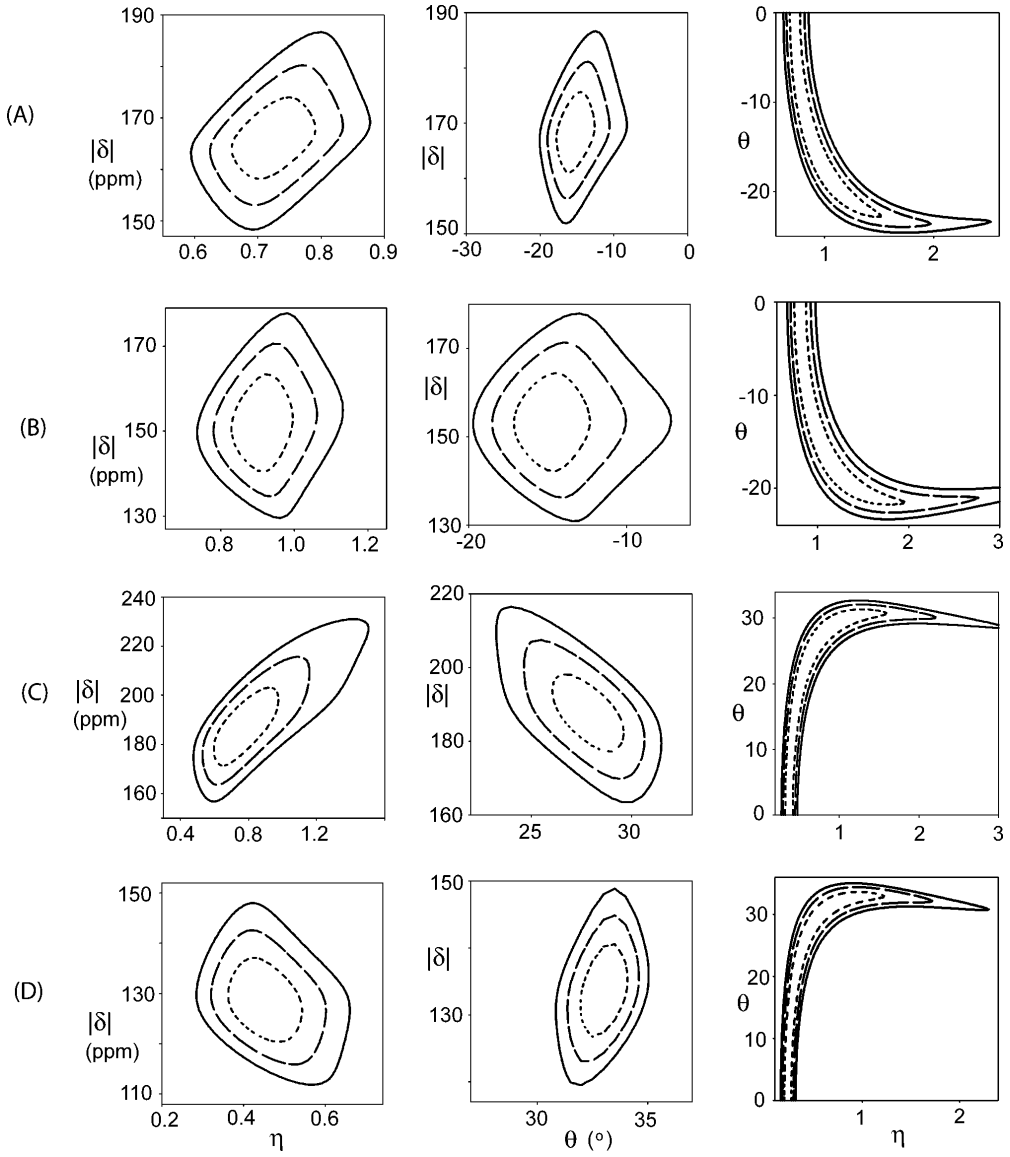

Figure 7. Contour plots of the total normalized error function when simultaneously fitting $(2R_2 - R_1)^{500\ \mathrm{MHz}}/(2R_2 - R_1)^{800\ \mathrm{MHz}}$ and $R_2/\Gamma_{C,CH}$ ratios for all carbons of a given type, assuming $\tau_c = 5.0$ ns and $D_{///}/D_{\perp} = 2.1$. Short-dashed, long-dashed, and solid contour lines are drawn at normalized χ values that are 1, 2, and 3 standard deviations above the minimum respectively. Three orthogonal cross sections through $|\delta|$, θ, η space are shown, taken at Stueber-and-Grant values for θ (left panel) and η (center panel), and at best-fitted values for $|\delta|$ (right panel). (A) Cross sections for adenine C2, at $\theta = -3°$, $\eta = 0.92$, and $|\delta| = 167$ ppm; (B) cytidine C5, at $\theta = -11°$, $\eta = 1.03$, and $|\delta| = 152.5$ ppm; (C) cytidine and thymidine C6, at $\theta = 27°$, $\eta = 0.83$, and $|\delta| = 186.5$ ppm; (D) adenine and guanine C6, at $\theta = 27°$, $\eta = 1.02$, and $|\delta| = 131$ ppm. All CSA values are scaled relative to a dipolar interaction constant corresponding to a 1.104-Å C–H bond length.

Our results are in better agreement with the experimental data derived from polycrystalline solid-state NMR measurements on mononucleotides than with the results of quantum chemical calculations, which generally point to smaller values of $|\delta|$. They also qualitatively confirm recent findings by Schwalbe and Duchhardt,[3] who noted that literature CSA values did not yield reasonable order parameters when interpreting relaxation data in terms of base dynamics. As also suggested in their report and confirmed by our data, in particular, the effect of the CSA magnitude is closely coupled to the anisotropy of the diffusion tensor. The commonly used practice in analysis of ^{15}N relaxation data in proteins, where noncollinearity of the chemical shift tensor with the dipolar interaction and asymmetry of the chemical shift tensor are often ignored, tends to have a serious impact on extracted dynamics parameters when applied to nucleic acid base carbons. It is therefore recommended that the equations of Spiess be used during such analyses, taking into account both anisotropy of the rotational diffusion tensor, and the effect of an asymmetric chemical shift tensor, not coaligned with the dipolar interaction.

Acknowledgements

We thank Nico Tjandra and Shou-Lin Chang for a copy of their program to calculate relaxation rates for an anisotropic rotor, and Dennis Torchia (NIDCR) for valuable discussions. This work was supported by the Intramural Research Program of the NIDDK, NIH,

and by the Intramural Antiviral Target Program of the Office of the Director, NIH.

REFERENCES

1. Shajani Z, Varani G. *J. Mol. Biol.* 2005; **349**: 699.
2. Vallurupalli P, Kay LE. *J. Am. Chem. Soc.* 2005; **127**: 6893.
3. Schwalbe H, Duchhardt E. *J. Biomol. NMR* 2005; **32**: 295.
4. Hoogstraten CG, Wank JR, Pardi A. *Biochemistry* 2000; **39**: 9951.
5. Showalter SA, Baker NA, Tang CG, Hall K. *J. Biomol. NMR* 2005; **32**: 179.
6. Brutscher B, Boisbouvier J, Pardi A, Marion D, Simorre JP. *J. Am. Chem. Soc.* 1998; **120**: 11 845.
7. Boisbouvier J, Brutscher B, Simorre JP, Marion D. *J. Biomol. NMR* 1999; **14**: 241.
8. Williamson J, Boxer S. *Biochemistry* 1989; **28**: 2819.
9. Sitkoff D, Case DA. *Prog. Nucl. Magn. Reson. Spectrosc.* 1998; **32**: 165.
10. Stueber D, Grant DM. *J. Am. Chem. Soc.* 2002; **124**: 10 539.
11. Fiala R, Czernek J, Sklenar V. *J. Biomol. NMR* 2000; **16**: 291.
12. Kojima C, Ono A, Kainosho M, James TL. *J. Magn. Reson.* 1998; **135**: 310.
13. Parhami P, Fung BM. *J. Am. Chem. Soc.* 1985; **107**: 7304.
14. Duchardt E, Richter C, Reif B, Glaser SJ, Engels JW, Griesinger C, Schwalbe H. *J. Biomol. NMR* 2001; **21**: 117.
15. Roberts JE, Harbison GS, Munowitz MG, Herzfeld J, Griffin RG. *J. Am. Chem. Soc.* 1987; **109**: 4163.
16. Case DA. *J. Biomol. NMR* 1999; **15**: 95.
17. Hiyama Y, Niu C-H, Silverton JV, Bavoso A, Torchia DA. *J. Am. Chem. Soc.* 1988; **110**: 2378.
18. Ottiger M, Bax A. *J. Am. Chem. Soc.* 1998; **120**: 12 334.
19. Tjandra N, Wingfield P, Stahl S, Bax A. *J. Biomol. NMR* 1996; **8**: 273.
20. Wang CY, Rance M, Palmer AG. *J. Am. Chem. Soc.* 2003; **125**: 8968.
21. Delaglio F, Grzesiek S, Vuister GW, Zhu G, Pfeifer J, Bax A. *J. Biomol. NMR* 1995; **6**: 277.
22. Cavanagh J, Fairbrother WJ, Palmer AG, Skelton NJ. *Protein NMR Spectroscopy – Principles and Practice*. Academic Press: San Diego, 1995.
23. Farrow NA, Muhandiram R, Singer AU, Pascal SM, Kay CM, Gish G, Shoelson SE, Pawson T, Forman-Kay JD, Kay LE. *Biochemistry* 1994; **33**: 5984.
24. Spiess HW. *NMR Basic Princ. Prog.* 1978; **15**: 55.
25. Chang SL, Tjandra N. *J. Magn. Reson.* 2005; **174**: 43.
26. Peng JW, Wagner G. *J. Magn. Reson.* 1992; **98**: 308.
27. Lipari G, Szabo A. *J. Am. Chem. Soc.* 1982; **104**: 4546.
28. Boisbouvier J, Wu ZR, Ono A, Kainosho M, Bax A. *J. Biomol. NMR* 2003; **27**: 133.
29. Wu Z, Delaglio F, Tjandra N, Zhurkin VB, Bax A. *J. Biomol. NMR* 2003; **26**: 297.
30. Fushman D, Tjandra N, Cowburn D. *J. Am. Chem. Soc.* 1999; **121**: 8577.